Colloids and Surfaces B: Biointerfaces 245 (2025) 114338

Contents lists available at ScienceDirect

Colloids and Surfaces B: Biointerfaces

journal homepage: www.elsevier.com/locate/colsurfb

Metallic-based phthalocyanine nanoemulsions for photodynamic purging of ovarian tissue in leukemia patients

Saeid Moghassemi [a], Arezoo Dadashzadeh [a], Saba Nikanfar [a], Pejman Ghaffari-Bohlouli [b], Paulo Eduardo Narcizo de Souza [c], Amin Shavandi [b], Ricardo Bentes de Azevedo [d], Christiani A. Amorim [a,*]

[a] Pôle de Recherche en Physiopathologie de la Reproduction, Institut de Recherche Expérimentale et Clinique, Université Catholique de Louvain, Brussels, Belgium
[b] Université libre de Bruxelles (ULB), École polytechnique de Bruxelles, 3BIO-BioMatter, Avenue F.D. Roosevelt, 50 - CP 165/61, Brussels 1050, Belgium
[c] Laboratory of Electron Paramagnetic Resonance, Institute of Physics, University of Brasilia, Brasilia, Brazil
[d] Laboratory of Nanobiotechnology, Department of Genetics and Morphology, Institute of Biological Sciences, University of Brasília, Brasilia, DF, Brazil

ARTICLE INFO

Keywords:
Photodynamic therapy
Nanoemulsion
Nanomedicine
Cancer therapy
Ovarian transplantation
Leukemia

ABSTRACT

For cancer patients with a high risk of ovarian tissue metastasis, ovarian autotransplantation is not advised due to the potential spread of malignant cells. *Ex vivo* purging of ovarian fragments may offer a more suitable alternative for fertility restoration. Eradicating malignant cells should be done selectively without affecting follicles or ovarian stromal cells (SCs). As a clinically licensed method, photodynamic therapy (PDT) is a minimally invasive treatment to destroy cancer cells. This study evaluates the effectiveness of nanoemulsions (NE) containing two phthalocyanine photosensitizers; aluminum (III) phthalocyanine (AlPc) and zinc (II) phthalocyanine (ZnPc) in eliminating cancer cells. Human leukemic malignant (HL-60) and ovarian stromal cells (SCs) were treated with AlPc/ZnPc loaded NEs with or without diode laser irradiation. HL-60 leukemia cells in 2D culture were eliminated by treatment with 10 nM AlPc-NE or 0.1 μM ZnPc-NE, while no toxicity was observed in SCs. In 3D culture models, although the cells showed more resistance to the NEs as a result of limited oxygen and photosensitizer penetration, the treatment remained selective for cancer cells. These approaches have the potential to eliminate malignant cells from ovarian tissue fragments.

1. Introduction

Ovarian tissue cryopreservation and autotransplantation (OTCT) is a valuable option for fertility preservation for prepubescent girls and women who require immediate cancer treatment. This procedure allows for the cryopreservation of harvested ovarian tissue before cancer treatment and subsequent autotransplantation following patient remission, which facilitates the restoration of endocrine function and enhances the prospects of successful conception in the future [1,2]. Up to now, over 90 % of patients have demonstrated restoration of ovarian function, with over 200 documented live births resulting from this OTCT [3,4]. However, due to the high risk of contamination of ovarian tissue with malignant cells during OTCT, the technique is not recommended for patients with chronic myeloid leukemia (CML) or acute myeloid leukemia (AML), as this could result in the recurrence of the illness after autotransplantation [5–7]. There are several promising alternatives under development for restoring fertility in patients who are not suitable candidates for OTCT. These include *in vitro* ovarian follicle culture [6,8], the bioengineered artificial ovary [9–13], and malignancy purging from OTs before autotransplantation [3,14–17].

Photodynamic therapy (PDT) is emerging as a promising cancer treatment due to its minimally invasive nature and ability to target tumors precisely [18–20]. In this strategy, after a selective accumulation at a specific tumor location, photosensitizer (PS) molecules can be stimulated by laser irradiation at a specific wavelength with suitable energy density, causing cancer cells to be eliminated. Briefly, the excited PS produces $^1O_2$ and other reactive oxygen species (ROS) in the presence of oxygen, which induces the oxidation of different macromolecules and tumor cell death [21–24]. Aluminum phthalocyanine (AlPc) and zinc(II) phthalocyanine (ZnPc) which are two metal-based tetracarboxylic

* Correspondence to: Pôle de Recherche en Physiopathologie de la Reproduction, Institut de Recherche Expérimentale et Clinique, Université Catholique de Louvain, Avenue Hippocrate 54, bte B1.55.03, Brussels 1200, Belgium.
E-mail address: christiani.amorim@uclouvain.be (C.A. Amorim).

https://doi.org/10.1016/j.colsurfb.2024.114338
Received 17 September 2024; Received in revised form 9 October 2024; Accepted 24 October 2024
Available online 24 October 2024

phthalocyanine PSs have been shown different localization in cancer cells. While AlPc has a mitochondrial localization, ZnPc mainly accumulates in the Golgi apparatus [25].

Apart from PDT benefits, many PSs fail to achieve expectations due to downsides such as self-aggregation, poor bioavailability, and inadequate tissue penetration [26,27]. Over the last decades, there has been extreme interest in the application of nanoparticles in PDT, which have several advantages, such as increasing the biodistribution, using the enhanced permeability and retention (EPR) effect, enhancing bioavailability, and decreasing PSs' tendency to be aggregated in an aqueous solution [28,29]. Nanoemulsions (NEs), which are biphasic dispersion of two immiscible liquid droplets stabilized by an interfacial layer of emulsifiers, have proven potential to improve drug permeability through biological membranes. NEs can also be employed for PS encapsulation to increase PDT efficiency and overcome their constraints [30,31].

In our previous *in vitro* study, we investigated the use of free AlPc and ZnPc to identify the optimal light energy density and treatment protocol for PDT of human leukemia cell lines, with the lowest damage to isolated human ovarian cells [16]. The results demonstrated the potential of these PSs to eliminate malignant cells while preserving ovarian tissue. However, challenges such as self-aggregation, low bioavailability, and limited tissue penetration remain. NE formulations can help address these issues by preventing the self-aggregation of phthalocyanines, enhancing tissue penetration, and improving both stability and bioavailability. Therefore, this study aims to develop AlPc- and ZnPc-loaded NEs and evaluate their in vitro PDT efficacy in both 2D and 3D models. In this study, human leukemia and ovarian SCs were employed for 2D *in vitro* assays and HL-60 and ovarian SCs embedded PEGylated fibrin was used for the 3D *in vitro* assays.

2. Materials and methods

2.1. Preparation of AlPc-NEs and ZnPc-NE

AlPc-NE and ZnPc-NE were prepared using the Phase Inversion by Temperature (PIT) method [32–34]. Briefly, the mixture of surfactant and oil (SOmix), including 1.8 g of polyethylene glycol sorbitan monolaurate (TWEEN® 20, 93773, Sigma) and 0.6 g of mineral oil (M5904, Sigma), was mixed by stirring (5 min, room temperature). Afterward, 5 μmol of AlPc (362530, Sigma) or ZnPc (341169, Sigma) was mixed in 3 ml ethanol and added to the SOmix. Then, the ethanol was removed by stirring at 90°C for 15 min. After reaching room temperature, distilled water was added slowly (1 ml/min) and stirred (15 min, room temperature). The same method was employed to prepare blank NEs but without the addition of any PSs.

2.2. Characterization of AlPc-NE and ZnPc-NE

The dynamic light scattering (DLS) technique via Zetasizer Nano ZS (Malvern Instruments Limited, Worcestershire, UK) was employed to analyze the vesicle size, polydispersity index (PDI), and Zeta potential (ZP) of blank-NE, AlPc-NE, and ZnPc-NE. The nanoemulsions were kept at room temperature and to evaluate their storage stability, DLS was run immediately and periodically for six months after preparation of the nanoemulsions. Moreover, the morphology of Blank-NEs, AlPc-NEs, and ZnPc-NEs was investigated by transmission electron microscopy (TECNAI 10, Philips), operating at 80 kV [35]. All the experiments were performed in triplicate.

2.3. Human ovarian stromal cell isolation

The ovarian tissue biopsies were collected following permission from the Université Catholique de Louvain's Institutional Review Board in May 2019 for the use of the human ovarian cortex (IRB reference 2012/23MAR/125, registration number B403201213872). Minimum Essential Medium (MEM; 42360–024; Gibco, Netherlands) was used to transfer the dissected ovary to the laboratory at 4°C. The cortex was frozen using our standard method after the medullar section was removed [36]. After thawing [36], the ovarian SCs were isolated from the ovarian tissue [37]. The tissue was chopped using a tissue sectioner (McIlwain Tissue Chopper, Mickel Laboratory, UK) set to 0.5 mm, and then digested for 75 minutes at 37°C with Liberase DH (5401054001; Sigma-Aldrich, Belgium) and DNAse I (10104159001; Sigma-Aldrich). The enzymatic digestion was then inactivated by combining equal amounts of Dulbecco's phosphate-buffered saline (DPBS; Gibco; 14190144) with 10 % heat-inactivated fetal bovine serum (HI-FBS; 16140–071; Gibco). The suspension was then centrifuged after being filtered using 80 μm (NY8002500; Millipore, Belgium) and 30 μm (NY3002500; Millipore) nylon net filters (500 g, 10 min).

2.4. Cell culture

After centrifuging the isolated ovarian stromal cell, the pellet was resuspended in Dulbecco's modified Eagle's medium F-12 nutrition combination (DMEM/F12; Gibco; 21041–025) with 10 % HI FBS and 1 % antibiotic and antimycotic agents (AA; 15240–062, Gibco). For cell subculture, we used Accutase (A6964; Sigma), and the passage-five ovarian SCs were seeded in a 96-well plate (Sarstedt, Germany) 24 h before the *in vitro* analysis (2×10^4 cells/well). On the other hand, a human leukemic malignant cell line (HL-60, 98070106, Sigma) was grown in RPMI-1640 media (61870–010, Gibco) supplemented with 10 % HI-FBS and 1 % AA. In a 96-well plate covered with poly-D-lysine (PDL; A3890401; Gibco), HL-60 cells were cultured (2×10^4 cells/well) for *in vitro* assays.

2.5. Cytocompatibility

The cytocompatibility of blank-NE was assessed by an *in vitro* test on human ovarian SCs. Briefly, SCs were cultured overnight in a 96-well plate (2×10^4 cells per well). Then, the medium was replaced by 1 μM blank NE in SCs culture medium (DMEM/F12 containing 10 % FBS and 1 % AA) and incubated for 2 h at 37°C. After one day of incubation, the cytocompatibility of blank NE was assessed by the cell viability assay using PrestoBlue™ HS and LIVE/DEAD™ Viability/Cytotoxicity Kit [17]. Normalization was performed using untreated cells, and wells with just medium were fixed as 100 % and 0 % viability, respectively. All the experiments were performed in triplicate.

2.6. Lipid peroxidation fluorescence staining

The Image-iT Lipid Peroxidation Kit (C10445; Invitrogen) was employed to measure the accumulation of lipid peroxide in cells. Briefly, SCs and HL-60 cells were seeded on μ-Slide 8 Well high plate (80806, ibidi) with a cell density of 3×10^4 cells/well and incubated for 24 h at 37 °C. After AlPC-NE and ZnPc-NE treatment or not (as control), the cells were incubated with the Image-iT Lipid Peroxidation sensor (10 μM) for 30 min at 37 °C. After staining with 10 μg/ml Hoechst 33342 (14533, Sigma), the cells were analyzed using confocal microscopy (LSM800; ZEISS). $^1O_2$ can affect unsaturated lipids, forming lipid hydroperoxide intermediates, which causes the probe to have a shift from red to green channel [38,39]. The lipid peroxidation rate was quantified using the following equation [40];

$$\textit{Lipid peroxidation rate}(\%) = \quad 100(FI)/(FI+TRI) \tag{1}$$

Where FI and TRI are respectively the fluorescence intensities of FITC and Texas Red measured using Image J software.

2.7. Intracellular ROS generation

The amount of ROS production in HL-60 cells was evaluated by

dichlorodihydrofluorescein diacetate (H2DCFDA, D399; Invitrogen), which can be oxidized to 2′,7′-dichlorofluorescein in the presence of ROS [41,42]. The H2DCFDA stock solution was made in DMSO (5 mM) and stored at −20°C. HL-60 cells were cultured in a PDL-coated glass-bottom 96-well plate (PBK96G-1.5–5-F; MatTek, USA) with a cell density of 1×10^4 cells/well for 24 h. Then, the cells were treated or not by the IC_{50} concentration of AlPc-NE or ZnPc-NE, they were washed with DPBS, and 20 μM H2DCFDA was added. After 30 min incubation, the cells were washed three times, and intracellular ROS generation was visualized using super-resolution 3D microscopy (3D Cell Explorer; Nanolive, Switzerland). Using ImageJ software, the generated ROS was measured to determine the average intracellular fluorescence intensity. Each pixel in an 8-bit image can have one of 256 values between 0 and 255, and RGB histograms display the frequency distribution of pixel values, the normalization was done using the highest and lowest pixel values as 100 % and 0 % intensity, respectively (n = 6).

2.8. 2D/3D PDT assay

Ovarian stromal and HL-60 cells were *in vitro* cultured in two- and three-dimensional structures for 24 h and 72 h, respectively. PEGylated fibrin with molar ratios of 10:1 was used to embed the cells with a cell density of 10^3 cells/μl [10]. Then, they were treated by AlPc-NE or ZnPc-NE with different concentrations (0, 0.0001, 0.0005, 0.001, 0.005, 0.01, 0.05, 0.1, 0.5, and 1 μM) for 2 h. Then, the medium was replaced and the cells were exposed or not to a 660 nm diode laser with the energy density of 10 J/cm^2 (11.15 mW/cm^2, 15 min) for AlPc-PDT groups and 50 J/cm^2 (18.59 mW/cm^2, 45 min) for ZnPc-PDT groups. Then, the plates were *in vitro* cultured for another 24 hours before cell viability analysis by LIVE/DEAD® cell staining and PrestoBlue™ assay [16]. The cell viability was also evaluated after five days post-PDT incubation to see any possible relapse. All the experiments were performed in triplicate.

2.9. Measurement of cell apoptosis

Cell-embedded PEGylated fibrin hydrogel was cultured in μ-slide eight-well ibiTreat dishes (80806, Ibidi) for 24 h. They were treated by AlPc-NE or ZnPc-NE with different concentrations (0, 0.01, 0.1, and 1 μM) using the same process described in the previous section. After 24 h, samples were washed with PBS and stained using an apoptosis detection kit (V13242, Molecular Probes, USA) that contains annexin V-FITC and propidium iodide (PI). Hoechst 33342 was added at a concentration of 20 μg/ml to count all the cells [43,44]. Hoechst (455 nm), Annexin V-FITC (FITC, 519 nm), and PI (674 nm) fluorescence were immediately observed under a confocal laser scanning microscope (Olympus, FV1000, Tokyo, Japan) and four categories of cells were distinguished: early apoptotic (annexin V-FITC-positive), dead (propidium iodide-positive), late apoptotic (double-positive), and viable (double-negative).

2.10. Statistical analysis

The quantitative data were presented as mean ± standard deviation (SD) and one-way ANOVA was used to statistically evaluate the data. Statistical significance was defined as a P value of less than 0.05. In graphs, the error bars represent a single sample SD.

3. Results

3.1. AlPc-NE and ZnPc-NE characterization

The size, ZP, and PDI of blank-NE, AlPc-NE, and ZnPc-NE were studied using DLS, which determines the Brownian motion diffusion of the particles and applies the Stokes-Einstein relation to determine the size and PDI [45]. Table 1 shows the DLS characteristics of the nanoemulsions. Due to their PDI lower than 0.2, these nanoemulsions could be classified as monodisperse nanoparticles, which means they had a low aggregation tendency (Fig. 1b1–3) [3,46].

Table 1
Particle size, PDI, and ZP of blank NE, AlPc-NE, and ZnPc-NE.

NPs	Size (nm)		PDI		ZP (mv)	
	Mean	±SD	Mean	±SD	Mean	±SD
Blank-NE	171.75	7.65	0.0615	0.0025	−18.10	0.60
AlPc-NE	180.25	1.05	0.0975	0.0075	−37.05	1.15
ZnPc-NE	176.85	0.55	0.0870	0.0040	−29.15	0.65

Abbreviations: Nanoparticles, NPs; Nanoemulsion, NE; Polydispersity index, PDI; Zeta potential, ZP; aluminum (III) phthalocyanine, AlPc; and zinc (II) phthalocyanine, ZnPc.

The ZP of AlPc-NE and ZnPc-NE were −37.05±1.15 and −29.15 ±0.65 mV, respectively (Fig. 1c2,c3). These NE characteristics are comparable with the NEs made by mineral oil and Pluronic F68 [47]. To assess their storage stability, the DLS study on blank NE, AlPc-NE, and ZnPc-NE was run for six months following preparation. The droplet size and PDI did not change during the stability study and the changes in the values of ZP were not significant (Fig. 2), indicating that the nanoemulsions could stay stable in distilled water during the storage time.

3.2. Dark toxicity of AlPc-NE and ZnPc-NE and blank-NE cytocompatibility

The potential photodynamic activity of AlPc-NE and ZnPc-NE on stromal and HL-60 cells was evaluated in the dark (Fig. 3a,b). Cells were incubated with different concentrations of AlPc-NE and ZnPc-NE (0.001–1 μM) for 2 h and their viability was assessed after 24 h. No significant difference was seen between the cell survival of different concentrations and both formulations had no dark cytotoxicity. Moreover, the toxicity of nanoemulsion components was studied by incubating blank-NEs with SCs with and without subsequent 660 nm laser irradiation (Fig. 3c,d). The blank-NE showed no cytotoxicity for SCs and did not cause significant phototoxicity, suggesting suitable cytocompatibility (Fig. 3d).

3.3. Intracellular ROS generation after AlPc-NE and ZnPc-NE treatment

Effective and constant intracellular ROS production to trigger oxidative stress is one of the most important factors influencing PDT anticancer effectiveness [48]. Once ROS forms, intracellular penetrated H2DCFDA could have been oxidized to DCF, which can be identified by a green fluorescence detector. The Nanolive fluorescence microscopy analysis of the untreated, AlPc-NE-treated, and ZnPc-NE-treated HL60 cells indicated that the IC_{50} concentration of both NEs causes a significant amount of ROS in the cells after the light exposure (Fig. 4).

3.4. Lipid peroxidation assays of AlPc-NE and ZnPc-NE

The lipid peroxidation fluorescence probe (BODIPY® C11) localizes throughout lipid membranes and has been employed to study the effect of ROS generation on lipid peroxidation. Intracellular lipid peroxidation levels in ovarian stromal and HL-60 cells were studied after the treatment by AlPc-NE and ZnPc-NE or not (as control) (Fig. 5a,b). The quantitative lipid peroxidation rate is depicted in Figs. 5c and 5d, revealing a substantial increase in lipid peroxidation in the treated HL-60 cells compared to the untreated cells. In contrast, there was no observable change in the peroxidation rate of SCs, regardless of treatment.

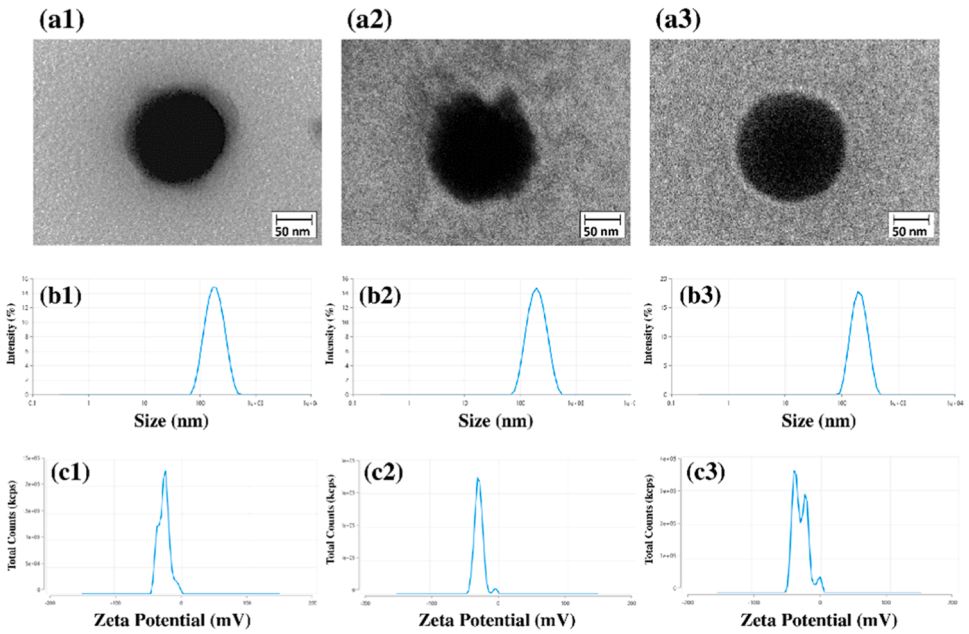

Fig. 1. Morphology, size distribution, and zeta potential of NEs. TEM images of blank-NEs (a1), AlPc-NEs (a2), and ZnPc-NEs (a3); the size and zeta potential distribution of freshly-synthetized blank-NEs (b1, c1), AlPc-NEs (b2, c2), and ZnPc-NEs (b3, c3).

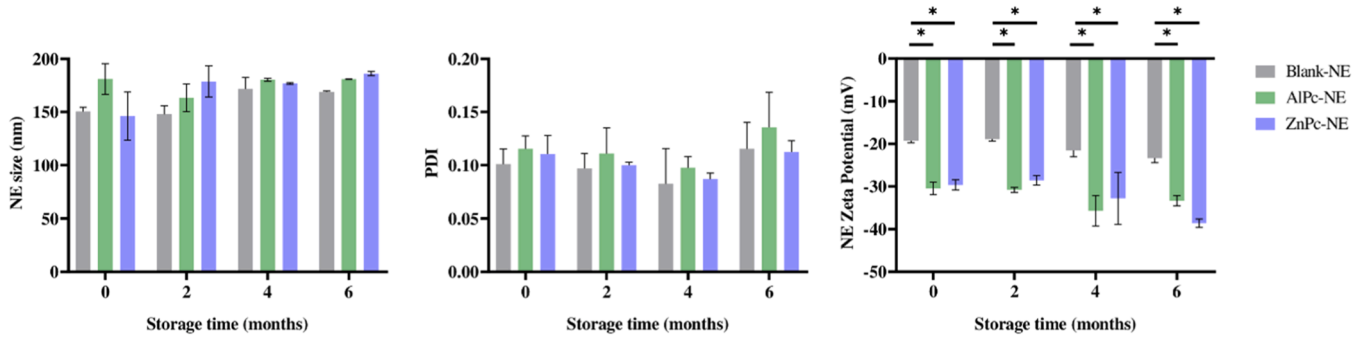

Fig. 2. Storage stability of the NEs. Size and PDI of the NEs just after preparation and 2, 4, and 6 months after the preparation (d); and NEs' zeta potential just after preparation and 2, 4, and 6 months after the preparation (e) (* $P<0.05$).

3.5. The PDT efficiency of AlPc-NE and ZnPc-NE to destroy leukemia cells

The efficiency and selectivity of the PDT approaches were evaluated by 2D (Figs. 6) and 3D (Fig. 7) *in vitro* assays. Stromal and HL-60 cells were incubated with different concentrations of AlPc-NE and ZnPc-NE (0.001–1 μM) for 2 h before laser irradiation. The results of the 2D *in vitro* assay revealed that while AlPc-NE and ZnPc-NE IC50 for HL-60 are 3 and 30 nM, their IC50 for SCs are 21 and 353 nM, respectively (Fig. 6a1,b1). In addition, while a complete eradication of HL-60 occurs starting from the concentration of 5 nM of AlPc-NE or 77 nM ZnPc-NE, the IC90 of these treatments on SCs are as high as 56 nM and 818 nM, respectively (Table 2). After five days of the treatment, there was no relapse of HL-60 cells and complete eradication was observed using the treatments of 10 nM AlPc-NE and 0.1 μM ZnPc-NE, while the same treatment showed no significant toxicity for SCs (Fig. 6a2,b2), demonstrating the selective eradication of cancer cells. These results were confirmed by consistent findings from the Live/Dead assay (Fig. 6c), where the 0.01 μM AlPc-NE and 0.1 μM ZnPc-NE could completely eradicate malignant cells, but the same treatments demonstrated minimal toxicity for SCs.

3D models, as more accurate artificial environments, have been exposed to different concentrations of the NEs to evaluate the effect of NEs transport, light penetration, and cell-ECM interaction on the PDT efficiency (Fig. 7). AlPc-NE has demonstrated a notable efficacy in purging malignancy, exhibiting 50 % inhibition of HL-60 at the concentration of 18.64 ± 1.13 nM while its IC_{50} on SCs is 61.91 ± 12.66 nM (Table 2). On the other hand, there was a significant phototoxicity of 1 μM ZnPc-NE for HL-60, and the same treatment caused no significant toxicity on SCs (Fig. 7b1,2). LIVE/DEAD assay also confirmed that SCs could survive the treatment up to 1 μM ZnPc-NE, while HL-60 cells were eliminated. The complete eradication of HL-60 and SCs after AlPc-NE PDT occurred at concentrations of 0.1 and 1 μM, respectively (Fig. 8a). The apoptotic assay revealed that both treatments invoke the apoptosis process to inhibit growth. Moreover, the secondary necrosis as a result of a complete apoptotic program could be visualized on HL-60 after the treatment by 1 μM of the NEs (Fig. 8b).

4. Discussion

In this study, AlPc and ZnPc have been loaded in nanoemulsions to improve some of their characteristics for pharmaceutical applications, such as bioavailability, biodistribution, pharmacokinetics, and tissue penetration [49]. It has been demonstrated by Tedesco et al. [30] that the PDT activity of AlPc can be enhanced up to 55 % by utilizing NEs, in comparison to the free form of the PS. Moreover, the stability and

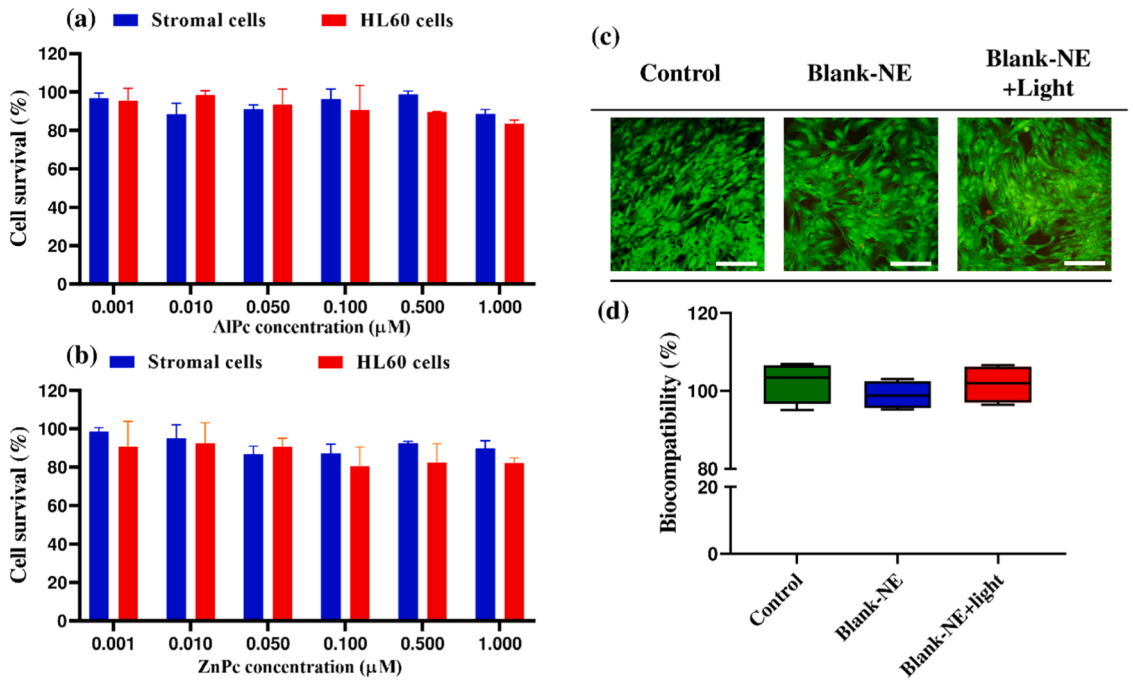

Fig. 3. Dark toxicity and cytocompatibility of NEs. Dark toxicity of metallic-based phthalocyanine-loaded nanoemulsions; AlPc-NE on human ovarian stromal and HL-60 cells (a), ZnPc-NE on human ovarian stromal and HL-60 cells (b). The cytocompatibility of blank-NE on human ovarian stromal with or without light irradiation (50 J/cm^2) using LIVE/DEAD® (c) and PrestoBlue™ (d) assays (scale bar: 200 μm).

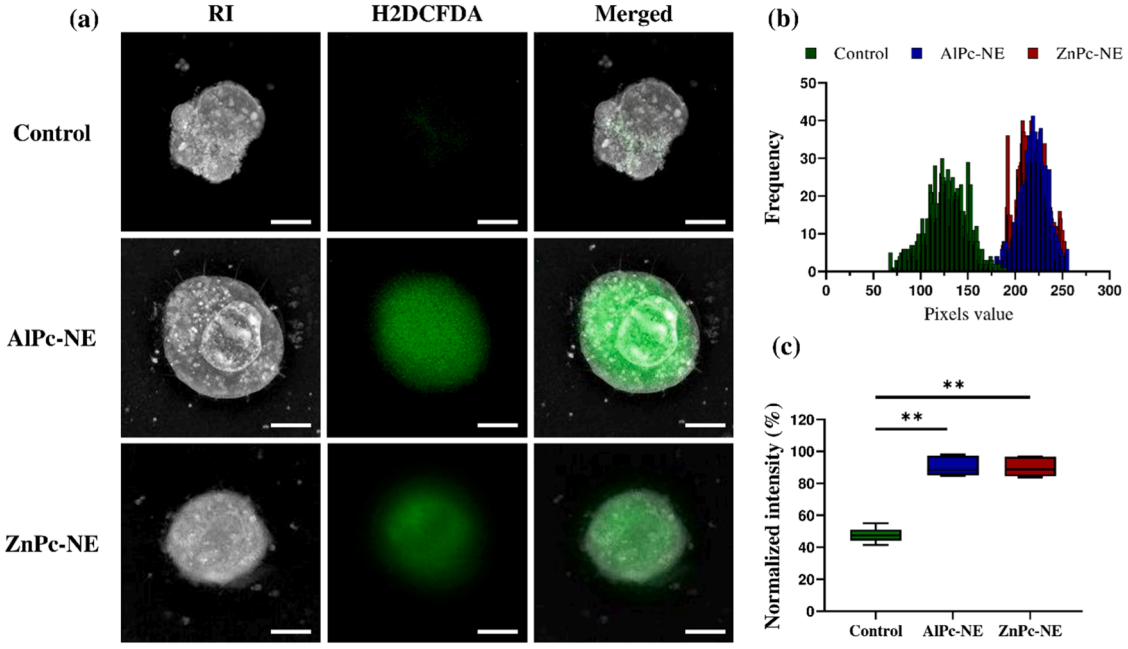

Fig. 4. ROS generation in HL-60 by AlPc-NE and ZnPc-NE before and after irradiation. ROS generation in untreated HL-60 cell (control), or after PDT by the IC_{50} concentration of AlPc-NE and ZnPc-NE (scale bar: 10 μm) (a), the histograms of the frequency distribution of intracellular green pixels value (b), and the normalized value of the green intensity in control, AlPc-NE treated or ZnPc-NE treated cells (c) (** $P<0.01$).

photobiological activity of phthalocyanines were found to be enhanced when they were incorporated in NEs [50].

The NEs in this study could be classified as monodisperse nanoparticles, due to their sharp size distribution and PDI lower than 0.2, showing their low aggregation tendency [3,46,51]. The ZP of AlPc-NE and ZnPc-NE were −37.05 ± 1.15 mV and −29.15 ± 0.65 mV, respectively. The ZP of NEs, determined by the measured particle's electrophoretic mobility, is crucial. NEs with a ZP below −25 mV are considered physically stable and capable of keeping the particle well suspended [49,52,53]. These NEs demonstrate comparable characteristics to those made with mineral oil and Pluronic F68, particularly in terms of size, PDI, and ZP [47]. The colloidal and photophysical stability of approaches in this study did not significantly vary over six months. Similarly, it has been reported that AlPc-NE could be stored for at least one year [54]. Moreover, Dalmolin et al. observed that the size, PDI, ZP, and pH of the ZnPc nanoemulsions remained stable throughout the

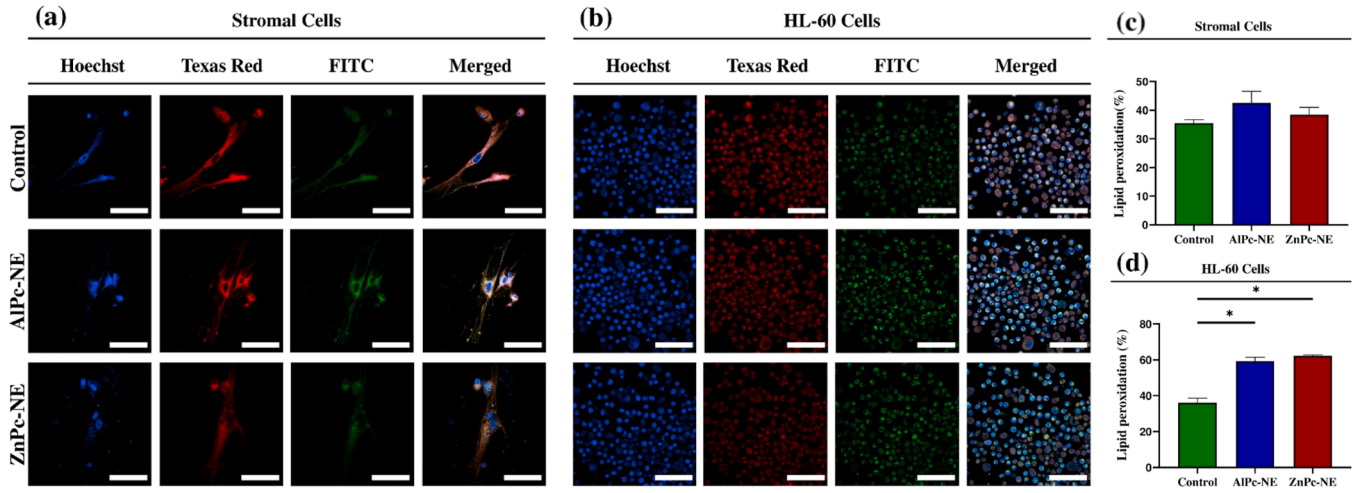

Fig. 5. Lipid peroxidation in SCs and HL-60 by AlPc-NE and ZnPc-NE before and after irradiation. Confocal microscopy imaging of the untreated, AlPc-NE-treated, and ZnPc-NE-treated SCs (a) and HL-60 cells (b) stained by the Lipid Peroxidation Kit and Hoechst (scale bar: 100 μm). Quantitative lipid peroxidation rate after different treatments on SCs (c) and HL-60 cells (d) (* $P<0.05$).

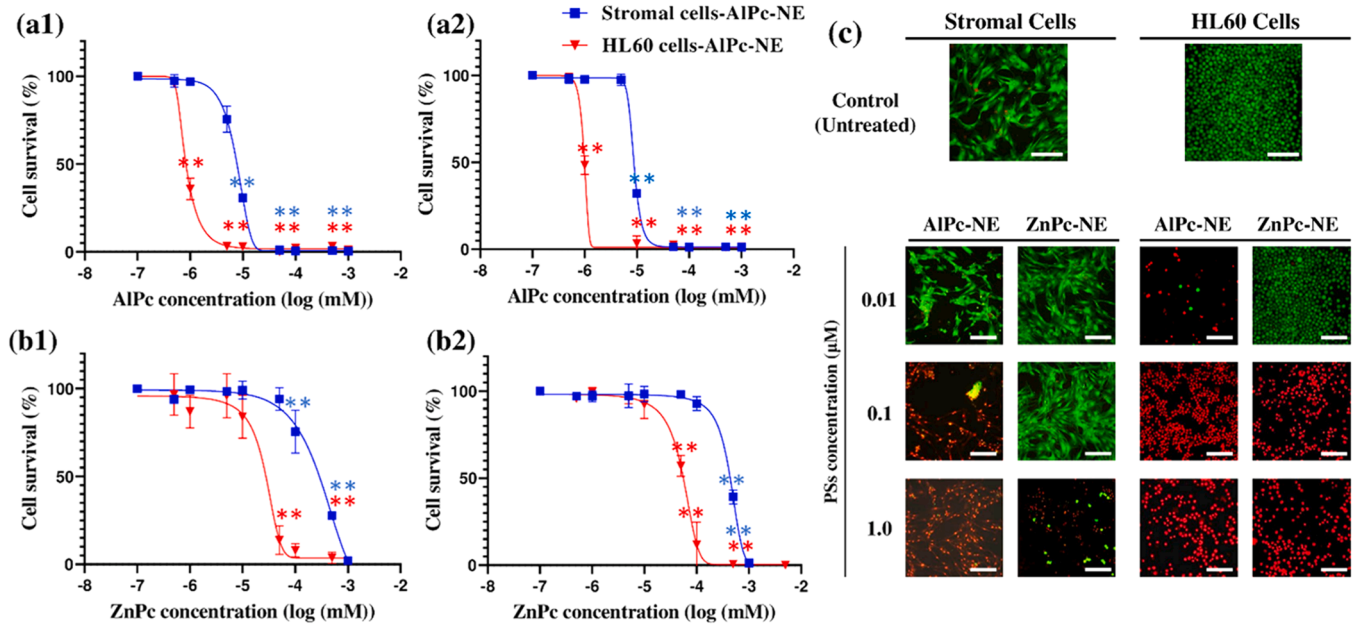

Fig. 6. PDT efficiency of AlPc-NE and ZnPc-NE in 2D *in vitro* models. Mitochondrial activity of ovarian stromal and HL-60 cells in 2D *in vitro* models after the treatment by AlPc-NE, 24 h (a1) or 5 days after PDT (a2), and ZnPc-NE 24 h (b1) or 5 days after PDT (b2). LIVE/DEAD assay of human ovarian stromal and HL-60 cells (c) without treatment or after treatment with different concentrations of AlPc-NE or ZnPc-NE (0.01, 0.1, and 1 μM) (scale bar: 200 μm) (** $P<0.01$).

30-day experiment [55].

For PDT to be effective, PSs need to be non-toxic in the dark. This ensures that only tissues exposed to light during treatment are affected by PDT [56]. In this study, it was found that both AlPc-NE and ZnPc-NE do not exhibit any toxicity on stromal and HL-60 cells when they are not exposed to light. Free AlPc and ZnPc demonstrated no toxicity for leukemia and ovarian SCs in the absence of light [16]. Similarly, liposomal AlPc and ZnPc have been reported to exhibit no significant dark toxicity for HeLa cervical carcinoma and human squamous carcinoma cells, even up to a concentration of 1 μM [57].

The blank-NE demonstrated cytocompatibility both with and without light exposure, which is an important finding, as it confirms that the components of the NE exhibit no in vitro toxicity. This suggests that the cell death observed after PDT with AlPc- or ZnPc-NE is solely due to ROS generation by the activated photosensitizers loaded in the nanoparticles. Notably, the cytocompatibility of blank-NE has also been established in various other cell types, including human breast adenocarcinoma MCF-7 cells [34] and murine breast adenocarcinoma 4T1 cells [33].

The NEs containing AlPc and ZnPc have been observed to induce intracellular ROS and lipid peroxidation. Due to the pre-existing oxidative stress in cancer cells, they are notably more susceptible to additional ROS damage from external agents. Consequently, the modulation of ROS levels has the potential to selectively eliminate cancer cells while mitigating adverse effects on normal cells [58–60]. A comprehensive understanding of the inherent variances between normal and cancer cells holds promise for advancing the development of more effective therapeutic interventions in preventing tumor progression.

Our research findings indicate that by using AlPc-NE and ZnPc-NE, we could completely eradicate malignant cells by 10 nM AlPc-NE and

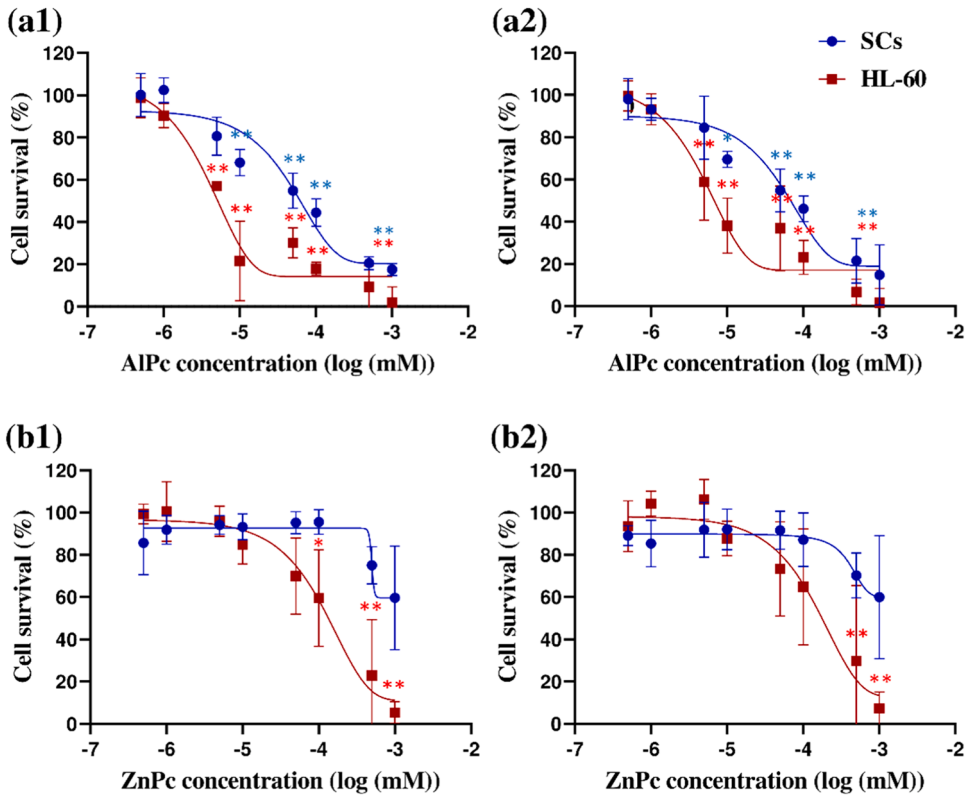

Fig. 7. PDT efficiency of AlPc-NE and ZnPc-NE in 3D *in vitro* models. Mitochondrial activity of ovarian stromal and HL-60 cells in 3D *in vitro* models after the treatment by AlPc-NE, 24 h (a1) or 5 days after PDT (a2), and ZnPc-NE 24 h (b1) or 5 days after PDT (b2) (* $P<0.05$, ** $P<0.01$, *** $P<0.001$).

Table 2
Antiproliferative activity of AlPc -NE exposed to the diode laser with the energy density of 10 J/cm^2 and ZnPc-NE with the energy density of 50 J/cm^2 laser exposure on 2D/3D *in vitro* cell culture models of SCs and HL-60.

In vitro models	PS	SCs		HL-60 cells	
		IC_{50} (nM) ± SD	IC_{90} (nM) ± SD	IC_{50} (nM) ± SD	IC_{90} (nM) ± SD
2D	AlPC-NE	21.14 ± 0.64	55.73 ± 0.30	2.78 ± 0.65	45.10 ± 1.17
	ZnPc-NE	352.70 ± 20.30	818.07 ± 1.70	30.15 ± 1.45	76.82 ± 5.12
3D	AlPC-NE	61.91 ± 12.66	>1000	18.64 ± 1.13	355.42 ± 120.91
	ZnPc-NE	851.78 ± 7.44	>1000	507.58 ± 11.41	927.87 ± 14.22

100 nM ZnPc-NE. In a study by Muehlmann et al. [54], the effect of AlPc-NE (λ: 660 nm, 25 J/cm^2) on human mammary adenocarcinoma resulted in a 50 % cytotoxic concentration of 3.0 nM and a 100 % cytotoxic concentration of 93.0 nM. Similarly, in another study, the IC_{50} of AlPc-NE-treated breast adenocarcinoma 4T1 cells was reported to range from 7.0 to 11.4 nM [33]. The NE-encapsulated formulation of AlPc and ZnPc demonstrated superior efficacy compared to the free forms [16]. This enhancement can be attributed to several key factors. First, encapsulating the photosensitizers within the nanoemulsion significantly improves their solubility and stability in aqueous environments, addressing the inherent hydrophobicity of AlPc and ZnPc. Additionally, the nanoemulsion enhances passive targeting through the EPR effect, allowing the nanoparticles to preferentially accumulate in tumor tissues due to the abnormal vascular architecture present in tumors. The increased surface-area-to-volume ratio of the nanoemulsion further contributes to more efficient cellular uptake and improved bioavailability. These combined factors result in higher concentrations of photosensitizers within the tumor microenvironment, ultimately leading to more effective PDT by generating more significant levels of ROS upon light activation [61,62].

The development of anticancer drugs using *in vitro* tests has always posed challenges. Recent advances in the biomedical sciences have significantly improved the accuracy of cell culture methods by incorporating 3D culture systems, such as cell-embedded scaffolds and microfluidics [63]. These 3D models allow for a more accurate assessment of therapeutic responses, drug penetration, anti-apoptotic signaling, multicellular resistance, and hypoxia, as they account for cell-cell and cell-matrix interactions [64]. Furthermore, the effectiveness of the PDT approach necessitates not only selectivity in 2D in vitro culture but also validation in 3D. This is especially critical in ovarian tissue, where a gradient PS penetration rate is observed during the PDT purging procedure, necessitating a targeted approach employing a variety of PS concentrations. Overdosing the PS may lead to dysfunctional tissue boundaries, while insufficient PS concentration may result in ineffective elimination of cancer cells within the deeper tissue regions, potentially leading to disease recurrence. In this study, a mechanically-optimized PEGylated fibrin hydrogel with molar ratios of 10:1 was used to embed the cells at a density of 10^3 cells/μl for the development of the 3D model. This model was employed to evaluate the efficiency of AlPc/ZnPc-NEs-based PDT more accurately [10]. Notably, higher drug resistance was observed in 3D culture models, possibly due to reduced penetration of PSs and light, compared to 2D models [65]. Moreover, since PDT is an oxygen-dependent therapy, its effect may be diminished in the central zone of the hydrogel, as 3D cell culture models typically exhibit lower oxygen concentrations [66].

In this study, we developed an AlPc/ZnPc-NEs-based PDT approach for ex vivo purging of ovarian tissue from malignant cells, with the goal of enabling safe transplantation. Table 3 highlights various ex vivo purging strategies used to eliminate malignant cells from ovarian tissue. For example, dexamethasone was ineffective at removing contaminating

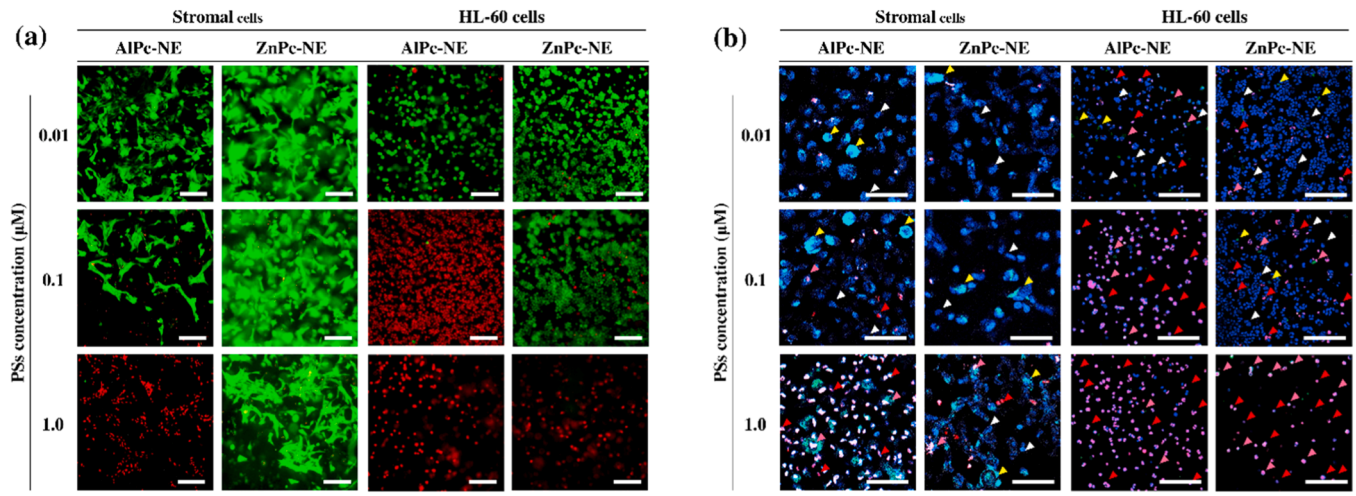

Fig. 8. Cell viability and apoptosis analyses. LIVE/DEAD assay of human ovarian stromal and HL-60 cells (a) after treatment with different concentrations of AlPc-NE or ZnPc-NE (0.01, 0.1, and 1 μM) (scale bar: 200 μm). The annexin V (green), Hoechst 33342 (blue), and PI (red) stained cells are shown in representative merged pictures (b) (scale bar: 200 μm). A white triangle denotes a viable cell, a yellow triangle early apoptosis, a pink triangle late apoptosis, and a red triangle dead cell.

Table 3
Ex vivo purging strategies to eradicate malignant cells from ovarian tissue.

PS	Cancer	Outcome	Ref.
Verteporfin, Imatinib	Rhabdomyosarcoma, leukemia	YAP/TAZ inhibition of cancer cells in ovarian tissue	[14]
Niosomal OR141	Leukemia	Eradication of the cancer cells in *ex vivo* tumor models	[3]
CMA	Ovarian cancer	Exhibition a high cytotoxicity in cancer cells with the minimum damage on non-cancer cells	[69]
DXM	Leukemia	DXM incubation before retransplantation fails to prevent leukemic cell reintroduction	[67]
Liposomal methylene blue	Ovarian cancer	Effective PDT for treating the ovarian malignancies	[70]
GSK1070916	Leukemia	Prevention of cancer cell reseeding through transplantation of ovarian tissue	[71]

Abbreviations: aluminum phthalocyanine, AlPc; zinc phthalocyanine, ZnPc; chlorin e_6-monoethylenediamine monoamide, CMA; yes-associated protein/transcriptional co-activator with PDZ-binding motif, YAP/TAZ; dexamethasone, DXM; Aurora B/C kinases inhibitor, GSK1070916.

acute lymphocytic leukemia cells from the ovarian cortex, as leukemia cells were still detectable after xenotransplantation of the purged tissue fragments to rodents [67]. Similarly, while the combination of Verteporfin and Imatinib successfully purged ovarian cortex tissue containing rhabdomyosarcoma and chronic myeloid leukemia, it was less effective against Ewing sarcoma and breast cancer cells, emphasizing the need for tailored purging regimens depending on the malignancy [14]. PDT-based purging, which exhibits light-dependent toxicity, can be applied to various cancer types and is considered safer than chemotherapy-based purging, as any remaining photosensitizer (PS) in the tissue post-transplantation does not cause unwanted toxicity in the body. Ex vivo purging relies on phototoxicity and is considered safer and more manageable. In contrast to niosomal OR141 [3], AlPc/ZnPc-NEs-based PDT demonstrated enhanced selectivity and stability and can be activated through irradiation with a lower absorption coefficient, allowing for deeper tissue penetration [68].

In conclusion, the AlPc-NE and ZnPc-NE have been developed as cytocompatible approaches with a high storage stability of up to six months, and they exhibit no dark toxicity. They showed a selective eradication of malignancy in both 2D and 3D *in vitro* studies which is one of the most vital requirements for the *ex vivo* PDT-purging application of malignant cells from ovarian fragments. Therefore, the NE approaches showed high potential to be used for ovarian tissue purging before autotransplantation. Further analysis is required to understand the underlying mechanisms of this selectivity, and it is imperative to conduct additional investigations to conclusively establish the efficacy of these approaches in purging *ex vivo* models both pre- and post-transplantation.

CRediT authorship contribution statement

Pejman Ghaffari-Bohlouli: Investigation. **Saba Nikanfar:** Investigation. **Arezoo Dadashzadeh:** Writing – original draft, Methodology, Investigation. **Saeid Moghassemi:** Writing – original draft, Visualization, Validation, Methodology, Investigation, Formal analysis, Data curation, Conceptualization. **Christiani A. Amorim:** Writing – review & editing, Supervision, Resources, Project administration, Funding acquisition. **Ricardo Bentes de Azevedo:** Writing – review & editing, Supervision. **Amin Shavandi:** Writing – review & editing, Resources. **Paulo de Souza:** Writing – review & editing, Resources.

Declaration of Competing Interest

The authors declare the following financial interests/personal relationships which may be considered as potential competing interests: Christiani A. Amorim reports financial support was provided by Louvain Foundation. Saba Nikanfar reports financial support was provided by FSR Belgium. If there are other authors, they declare that they have no known competing financial interests or personal relationships that could have appeared to influence the work reported in this paper.

Acknowledgments

This study was supported by grants from the Fonds de la Recherche Scientifique (grant FNRS-PDR T.0004.20 awarded to C.A.A. and FC 46825 awarded to S.M.) and FSR Incoming Post-doc Fellowship (grant IRECFSR23MOVEAND) awarded to S.N.

Data Availability

Data will be made available on request.

References

[1] J. Donnez, M.-M. Dolmans, Fertility preservation in women, N. Engl. J. Med. 377 (17) (2017) 1657–1665.
[2] E.C.R. Leonel, C.M. Lucci, C.A. Amorim, Cryopreservation of human ovarian tissue: a review, Transfus. Med. Hemother. 46 (3) (2019) 173–181.
[3] S. Moghassemi, A. Dadashzadeh, A. Camboni, O. Feron, R.B. Azevedo, C. A. Amorim, Ex vivo purging of cancer cells from ovarian tissue using photodynamic therapy: a novel strategy to restore fertility in leukemia patients, Hum. Reprod. Open 2023 (2) (2023) hoad005.
[4] M.-M. Dolmans, J. Donnez, Fertility preservation in women for medical and social reasons: oocytes vs ovarian tissue, Best. Pract. Res. Clin. Obstet. Gynaecol. (2020).
[5] M.C. Chiti, M.-M. Dolmans, L. Mortiaux, F. Zhuge, E. Ouni, P.A.K. Shahri, E. Van Ruymbeke, S.-D. Champagne, J. Donnez, C.A. Amorim, A novel fibrin-based artificial ovary prototype resembling human ovarian tissue in terms of architecture and rigidity, J. Assist. Reprod. Genet. 35 (1) (2018) 41–48.
[6] M. McLaughlin, D. Albertini, W. Wallace, R. Anderson, E. Telfer, Metaphase II oocytes from human unilaminar follicles grown in a multi-step culture system, MHR: Basic Sci. Reprod. Med. 24 (3) (2018) 135–142.
[7] D. Meirow, Fertility preservation in cancer patients using stored ovarian tissue: clinical aspects, Curr. Opin. Endocrinol., Diabetes Obes. 15 (6) (2008) 536–547.
[8] E.E. Telfer, M.B. Zelinski, Ovarian follicle culture: advances and challenges for human and nonhuman primates, Fertil. Steril. 99 (6) (2013) 1523–1533.
[9] C.A. Amorim, A. Shikanov, The artificial ovary: current status and future perspectives, Future Oncol. 12 (19) (2016) 2323–2332.
[10] A. Dadashzadeh, S. Moghassemi, C. Amorim, Evaluation of PEGylated fibrin as a three-dimensional biodegradable scaffold for ovarian tissue engineering, Mater. Today Chem. 22 (2021) 100626.
[11] A. Dadashzadeh, S. Moghassemi, A. Shavandi, C.A. Amorim, A review on biomaterials for ovarian tissue engineering, Acta Biomater. 135 (2021) 48–63.
[12] H. Jafari, A. Dadashzadeh, S. Moghassemi, P. Zahedi, C.A. Amorim, A. Shavandi, Ovarian cell encapsulation in an enzymatically crosslinked silk-based hydrogel with tunable mechanical properties, Gels 7 (3) (2021) 138.
[13] A. Dadashzadeh, S. Moghassemi, C.A. Amorim, Bioprinting of a liposomal oxygen-releasing scaffold for ovary tissue engineering, Tissue Eng. Part A (2024).
[14] C.L. Mulder, L.L. Eijkenboom, C.C. Beerendonk, D.D. Braat, R. Peek, Enhancing the safety of ovarian cortex autotransplantation: cancer cells are purged completely from human ovarian tissue fragments by pharmacological inhibition of YAP/TAZ oncoproteins, Hum. Reprod. 34 (3) (2019) 506–518.
[15] L. Eijkenboom, C. Mulder, B. van der Reijden, N. van Mello, J. van Leersum, T. Koorenhof-Scheele, D. Braat, C. Beerendonk, R. Peek, Purging human ovarian cortex of contaminating leukaemic cells by targeting the mitotic catastrophe signalling pathway, J. Assist. Reprod. Genet. (2021) 1–18.
[16] S. Moghassemi, A. Dadashzadeh, P.E.N. de Souza, R.B. Azevedo, C.A. Amorim, AlPc/ZnPc-based oncological photodynamic therapy for a selective eradication of leukemic cells from ovarian tissue, Photo Photodyn. Ther. 36 (2021) 102555.
[17] S. Moghassemi, A. Dadashzadeh, A. Camboni, O. Feron, R.B. Azevedo, C. A. Amorim, Photodynamic therapy using OR141-loaded nanovesicles for eradication of leukemic cells from ovarian tissue, Photo Photodyn. Ther. 40 (2022) 103139.
[18] U. Chilakamarthi, L. Giribabu, Photodynamic therapy: past, present and future, Chem. Rec. 17 (8) (2017) 775–802.
[19] P. Lehmann, Side effects of topical photodynamic therapy, Der Hautarzt; Z. fur Dermatol., Venerol., und Verwandte-.-. Geb. 58 (7) (2007) 597–603.
[20] S. Kwiatkowski, B. Knap, D. Przystupski, J. Saczko, E. Kędzierska, K. Knap-Czop, J. Kotlińska, O. Michel, K. Kotowski, J. Kulbacka, Photodynamic therapy–mechanisms, photosensitizers and combinations, Biomed. Pharmacother. 106 (2018) 1098–1107.
[21] S. Moghassemi, A. Dadashzadeh, R.B. de Azevedo, C.A. Amorim, Secure transplantation by tissue purging using photodynamic therapy to eradicate malignant cells, J. Photochem. Photobiol. B: Biol. (2022) 112546.
[22] S.K. Sharma, L.Y. Chiang, M.R. Hamblin, Photodynamic therapy with fullerenes in vivo: reality or a dream? Nanomedicine 6 (10) (2011) 1813–1825.
[23] M.G. Mokwena, C.A. Kruger, M.-T. Ivan, A. Heidi, A review of nanoparticle photosensitizer drug delivery uptake systems for photodynamic treatment of lung cancer, Photo Photodyn. Ther. 22 (2018) 147–154.
[24] T.J. Dougherty, C.J. Gomer, B.W. Henderson, G. Jori, D. Kessel, M. Korbelik, J. Moan, Q. Peng, Photodynamic therapy, JNCI: J. Natl. Cancer Inst. 90 (12) (1998) 889–905.
[25] Á. Juarranz, P. Jaén, F. Sanz-Rodríguez, J. Cuevas, S. González, Photodynamic therapy of cancer. Basic principles and applications, Clin. Transl. Oncol. 10 (3) (2008) 148–154.
[26] N. Düzgüneş, J. Piskorz, P. Skupin-Mrugalska, T. Goslinski, J. Mielcarek, K. Konopka, Photodynamic therapy of cancer with liposomal photosensitizers, Ther. Deliv. 9 (11) (2018) 823–832.
[27] A. Roby, S. Erdogan, V.P. Torchilin, Solubilization of poorly soluble PDT agent, meso-tetraphenylporphin, in plain or immunotargeted PEG-PE micelles results in dramatically improved cancer cell killing in vitro, Eur. J. Pharm. Biopharm. 62 (3) (2006) 235–240.
[28] J. Qian, D. Wang, F. Cai, Q. Zhan, Y. Wang, S. He, Photosensitizer encapsulated organically modified silica nanoparticles for direct two-photon photodynamic therapy and in vivo functional imaging, Biomaterials 33 (19) (2012) 4851–4860.
[29] J. Liu, Y. Yin, L. Yang, B. Lu, Z. Yang, W. Wang, R. Li, Nucleus-Targeted Photosensitizer Nanoparticles for Photothermal and Photodynamic Therapy of Breast Carcinoma, Int. J. Nanomed. 16 (2021) 1473.
[30] A.C. Tedesco, E.P. Silva, C.C. Jayme, H.L. Piva, L.P. Franchi, Cholesterol-rich nanoemulsion (LDE) as a novel drug delivery system to diagnose, delineate, and treat human glioblastoma, Mater. Sci. Eng.: C. 123 (2021) 111984.
[31] Y. Zhang, Y. Liao, Q. Tang, J. Lin, P. Huang, Biomimetic nanoemulsion for synergistic photodynamic-immunotherapy against hypoxic breast tumor, Angew. Chem. Int. Ed. 60 (19) (2021) 10647–10653.
[32] V. Monge-Fuentes, L.A. Muehlmann, J.P.F. Longo, J.R. Silva, M.L. Fascineli, P. de Souza, F. Faria, I.A. Degterev, A. Rodriguez, F.P. Carneiro, Photodynamic therapy mediated by acai oil (Euterpe oleracea Martius) in nanoemulsion: a potential treatment for melanoma, J. Photochem. Photobiol. B: Biol. 166 (2017) 301–310.
[33] M.C. Rodrigues, L.G. Vieira, F.H. Horst, E.C. de Araújo, R. Ganassin, C. Merker, T. Meyer, J. Böttner, T. Venus, J.P.F. Longo, Photodynamic therapy mediated by aluminium-phthalocyanine nanoemulsion eliminates primary tumors and pulmonary metastases in a murine 4T1 breast adenocarcinoma model, J. Photochem. Photobiol. B: Biol. 204 (2020) 111808.
[34] L.A. Muehlmann, M.C. Rodrigues, J.P.F. Longo, M.P. Garcia, K.R. Py-Daniel, A. B. Veloso, P.E.N. de Souza, S.W. da Silva, R.B. Azevedo, Aluminium-phthalocyanine chloride nanoemulsions for anticancer photodynamic therapy: Development and in vitro activity against monolayers and spheroids of human mammary adenocarcinoma MCF-7 cells, J. Nanobiotechnol. 13 (2015) 1–11.
[35] Y. Li, Y. Zhang, F. Qiu, Z. Qiu, Proteomic identification of exosomal LRG1: a potential urinary biomarker for detecting NSCLC, Electrophoresis 32 (15) (2011) 1976–1983.
[36] M. Gallardo, F. Paulini, A. Corral, M. Balcerzyk, C.M. Lucci, J. Ambroise, M. Merola, L. Fernandez-Maza, R. Risco, M.-M. Dolmans, Evaluation of a new freezing protocol containing 20% dimethyl sulphoxide concentration to cryopreserve human ovarian tissue, Reprod. Biomed. Online 37 (6) (2018) 653–665.
[37] P. Asiabi, M.-M. Dolmans, J. Ambroise, A. Camboni, C. Amorim, In vitro differentiation of theca cells from ovarian cells isolated from postmenopausal women, Hum. Reprod. 35 (12) (2020) 2793–2807.
[38] E. Pap, G. Drummen, V. Winter, T. Kooij, P. Rijken, K. Wirtz, J. Op den Kamp, W. Hage, J. Post, Ratio-fluorescence microscopy of lipid oxidation in living cells using C11-BODIPY581/591, FEBS Lett. 453 (3) (1999) 278–282.
[39] D.K. Adigbli, H. Pye, J. Seebaluck, M. Loizidou, A.J. MacRobert, The intracellular redox environment modulates the cytotoxic efficacy of single and combination chemotherapy in breast cancer cells using photochemical internalisation, RSC Adv. 9 (44) (2019) 25861–25874.
[40] D.V. Sakharov, E.D.R. Elstak, B. Chernyak, K.W.A. Wirtz, Prolonged lipid oxidation after photodynamic treatment. Study with oxidation-sensitive probe C11-BODIPY581/591, FEBS Lett. 579 (5) (2005) 1255–1260.
[41] Q. Li, W. Li, H. Di, L. Luo, C. Zhu, J. Yang, X. Yin, H. Yin, J. Gao, Y. Du, A photosensitive liposome with NIR light triggered doxorubicin release as a combined photodynamic-chemo therapy system, J. Control. Release 277 (2018) 114–125.
[42] A. Grebinyk, S. Grebinyk, S. Prylutska, U. Ritter, O. Matyshevska, T. Dandekar, M. Frohme, C60 fullerene accumulation in human leukemic cells and perspectives of LED-mediated photodynamic therapy, Free Radic. Biol. Med. 124 (2018) 319–327.
[43] Q. Miao, L.-L. Bi, X. Li, S. Miao, J. Zhang, S. Zhang, Q. Yang, Y.-H. Xie, J. Zhang, S.-W. Wang, Anticancer effects of bufalin on human hepatocellular carcinoma HepG2 cells: roles of apoptosis and autophagy, Int. J. Mol. Sci. 14 (1) (2013) 1370–1382.
[44] L. Szoka, E. Karna, K. Hlebowicz-Sarat, J. Karaszewski, S. Boryczka, J.A. Palka, Acetylenic derivative of betulin induces apoptosis in endometrial adenocarcinoma cell line, Biomed. Pharmacother. 95 (2017) 429–436.
[45] S. Bhattacharjee, DLS and zeta potential–what they are and what they are not? J. Control. Release 235 (2016) 337–351.
[46] P. Singh, J. Bodycomb, B. Travers, K. Tatarkiewicz, S. Travers, G.R. Matyas, Z. Beck, Particle size analyses of polydisperse liposome formulations with a novel multispectral advanced nanoparticle tracking technology, Int. J. Pharm. 566 (2019) 680–686.
[47] K.-S. Liu, K. Sung, S.A. Al-Suwayeh, M.-C. Ku, C.-C. Chu, J.-J. Wang, J.-Y. Fang, Enhancement of transdermal apomorphine delivery with a diester prodrug strategy, Eur. J. Pharm. Biopharm. 78 (3) (2011) 422–431.
[48] M. Dewaele, W. Martinet, N. Rubio, T. Verfaillie, P.A. de Witte, J. Piette, P. Agostinis, Autophagy pathways activated in response to PDT contribute to cell resistance against ROS damage, J. Cell. Mol. Med. 15 (6) (2011) 1402–1414.
[49] S. Moghassemi, A. Dadashzadeh, R.B. Azevedo, C.A. Amorim, Nanoemulsion applications in photodynamic therapy, J. Control. Release 351 (2022) 164–173.
[50] L.Bd.O. de Siqueira, V. da Silva Cardoso, I.A. Rodrigues, A.L. Vazquez-Villa, E. P. Dos Santos, Bd.C.L.R. Guimarães, Cd.S.C. Coutinho, A.B. Vermelho, E.R. Junior, Development and evaluation of zinc phthalocyanine nanoemulsions for use in photodynamic therapy for Leishmania spp, Nanotechnology 28 (6) (2017) 065101.
[51] S. Moghassemi, A. Dadashzadeh, H. Jafari, P. Ghaffari-Bohlouli, A. Shavandi, C. A. Amorim, Liposomal oxygen-generating hydrogel for enhancing cell survival under hypoxia condition, Colloids Surf. B: Biointerfaces 231 (2023) 113562.
[52] V.R. Patel, Y. Agrawal, Nanosuspension: an approach to enhance solubility of drugs, J. Adv. Pharm. Technol. Res. 2 (2) (2011) 81.
[53] P. Thanasekaran, C.-H. Chu, S.-B. Wang, K.-Y. Chen, H.-D. Gao, M.M. Lee, S.-S. Sun, J.-P. Li, J.-Y. Chen, J.-K. Chen, Lipid-wrapped upconversion nanoconstruct/photosensitizer complex for near-infrared light-mediated photodynamic therapy, ACS Appl. Mater. Interfaces 11 (1) (2018) 84–95.
[54] L.A. Muehlmann, M.C. Rodrigues, J.P.F. Longo, M.P. Garcia, K.R. Py-Daniel, A. B. Veloso, P.E.N. de Souza, S.W. da Silva, R.B. Azevedo, Aluminium-phthalocyanine chloride nanoemulsions for anticancer photodynamic therapy:

Development and in vitro activity against monolayers and spheroids of human mammary adenocarcinoma MCF-7 cells, J. Nanobiotechnol. 13 (1) (2015) 1–11.
[55] L.F. Dalmolin, R.F.V. Lopez, Nanoemulsion as a Platform for Iontophoretic Delivery of Lipophilic Drugs in Skin Tumors, Pharmaceutics 10 (4) (2018) 214.
[56] M.R. Detty, S.L. Gibson, S.J. Wagner, Current clinical and preclinical photosensitizers for use in photodynamic therapy, J. Med. Chem. 47 (16) (2004) 3897–3915.
[57] J. Young, M. Yee, H. Kim, J. Cheung, T. Chino, N. Düzgüneş, K. Konopka, Phototoxicity of liposomal Zn-and Al-phthalocyanine against cervical and oral squamous cell carcinoma cells in vitro, Med. Sci. Monit. Basic Res. 22 (2016) 156.
[58] G. Barrera, Oxidative stress and lipid peroxidation products in cancer progression and therapy, Int. Sch. Res. Not. 2012 (2012).
[59] H. Pelicano, D. Carney, P. Huang, ROS stress in cancer cells and therapeutic implications, Drug Resist. Updates 7 (2) (2004) 97–110.
[60] P.T. Schumacker, Reactive oxygen species in cancer cells: live by the sword, die by the sword, Cancer Cell 10 (3) (2006) 175–176.
[61] J.N. Sharma, D.K. Pattadar, B.P. Mainali, F.P. Zamborini, Size determination of metal nanoparticles based on electrochemically measured surface-area-to-volume ratios, Anal. Chem. 90 (15) (2018) 9308–9314.
[62] D. Kalyane, N. Raval, R. Maheshwari, V. Tambe, K. Kalia, R.K. Tekade, Employment of enhanced permeability and retention effect (EPR): nanoparticle-based precision tools for targeting of therapeutic and diagnostic agent in cancer, Mater. Sci. Eng.: C. 98 (2019) 1252–1276.
[63] A. Shehzad, V. Ravinayagam, H. AlRumaih, M. Aljafary, D. Almohazey, S. Almofty, N.A. Al-Rashid, E.A. Al-Suhaimi, Application of three-dimensional (3D) tumor cell culture systems and mechanism of drug resistance, Curr. Pharm. Des. 25 (34) (2019) 3599–3607.
[64] L. Mohammad-Hadi, A.J. MacRobert, M. Loizidou, E. Yaghini, Photodynamic therapy in 3D cancer models and the utilisation of nanodelivery systems, Nanoscale 10 (4) (2018) 1570–1581.
[65] Y. Yang, X. Yang, J. Zou, C. Jia, Y. Hu, H. Du, H. Wang, Evaluation of photodynamic therapy efficiency using an in vitro three-dimensional microfluidic breast cancer tissue model, Lab a Chip 15 (3) (2015) 735–744.
[66] L. Markova, V. Novohradsky, J. Kasparkova, J. Ruiz, V. Brabec, Dipyridophenazine iridium (III) complex as a phototoxic cancer stem cell selective, mitochondria targeting agent, Chem. -Biol. Interact. 360 (2022) 109955.
[67] C. Díaz-García, S. Herraiz, E. Such, Md.M. Andrés, E. Villamón, E. Mayordomo-Aranda, J.V. Cervera, M.A. Sanz, A. Pellicer, Dexamethasone does not prevent malignant cell reintroduction in leukemia patients undergoing ovarian transplant: risk assessment of leukemic cell transmission by a xenograft model, Hum. Reprod. 34 (8) (2019) 1485–1493.
[68] S. Moghassemi, A. Dadashzadeh, R.B. de Azevedo, C.A. Amorim, Secure transplantation by tissue purging using photodynamic therapy to eradicate malignant cells, J. Photochem. Photobiol. B: Biol. 234 (2022) 112546.
[69] B.A. Goff, M. Bamberg, T. Hasan, Photoimmunotherapy of human ovarian carcinoma cells ex vivo, Cancer Res. 51 (18) (1991) 4762–4767.
[70] M. Ismail, U. Torsten, C. Dressler, J. Diederichs, S. Hüske, H. Weitzel, H.-P. Berlien, Photodynamic therapy of malignant ovarian tumours cultivated on CAM, Lasers Med. Sci. 14 (2) (1999) 91–96.
[71] L. Eijkenboom, C. Mulder, B. van der Reijden, N. van Mello, J. van Leersum, T. Koorenhof-Scheele, D. Braat, C. Beerendonk, R. Peek, Purging human ovarian cortex of contaminating leukaemic cells by targeting the mitotic catastrophe signalling pathway, J. Assist. Reprod. Genet. 38 (2021) 1571–1588.